metals

MDPI

Article

Influence of Intermetallic Particles on the Corrosion Properties of Extruded ZK60 Mg Alloy Containing Cu

Soo-Min Baek, Beomcheol Kim and Sung Soo Park *

School of Materials Science and Engineering, Ulsan National Institute of Science and Technology, Ulsan 44919, Korea; bsm78914@unist.ac.kr (S.-M.B.); kbc1012@unist.ac.kr (B.K.)

* Correspondence: sspark@unist.ac.kr; Tel.: +82-52-217-2328

Received: 16 April 2018; Accepted: 5 May 2018; Published: 7 May 2018

Abstract: The microstructure and corrosion behavior of the extruded ZK60 Mg alloys with different Cu content were comparatively investigated. The ZK60 alloy had a microstructure consisting of α-Mg grains with intermetallic $MgZn_2$ and Zn_2Zr_3 particles. The addition of 1 wt % Cu resulted in the additional presence of CuMgZn particles. In a 0.6 M NaCl solution at 25 °C, the corrosion rate of the alloy with the added Cu appeared to be about 16% faster than that of the alloy without the addition of Cu. The factors affecting the degraded corrosion resistance of the Cu-added ZK60 alloy are discussed.

Keywords: magnesium alloy; extrusion; intermetallic particle; corrosion

1. Introduction

The development of high performance and cost-effective Mg alloy extrusions is of necessity in order to cope with the growing need for lightweight components in automobiles [1]. However, few Mg alloy extrusions satisfy the property and cost requirements of the automobile industry at present [2]. In most cases, this is due to an incompatible situation as high strength Mg alloys, which usually contain a large amount of alloying elements, show low extrusion speed since such alloys are susceptible to hot-cracking at high extrusion speeds where excessive frictional heat is generated [3]. Generally, the hot-cracking results from the incipient melting of second-phase particles in the microstructure [4]. Thus, it is believed that high strength Mg alloy extrusions with a sound surface condition can be obtained at faster speeds via the modification of their alloy compositions in order to retain more thermally stable second-phase particles, thereby realizing better resistance against hot-cracking.

One of the promising alloying elements for this purpose is Cu, which has been used to raise the incipient melting temperature of second-phase particles, especially in the Mg–Zn-based alloy system. This has permitted the use of higher solution treatment temperatures and hence, enabled an enhanced age hardening response [5]. Recently, it has been shown that the tensile strength level of the extruded Mg–Zn-based alloys is significantly elevated by addition of Cu [6]. This reveals the potential of Cu as an alloying element that is also capable of improving the mechanical properties of Mg alloy extrusions. However, most previous studies on Cu-containing Mg–Zn-based alloys have been conducted with a particular emphasis on their mechanical properties and few reports on their corrosion behavior have been made available thus far [6–10]. Since Cu is known to be one of the most harmful elements in terms of the corrosion resistance of Mg [11–14], investigating the corrosion behavior of the Cu-added Mg–Zn-based alloys and their mechanical properties is necessary. In the present study, the commercial Mg–6Zn–0.5Zr alloys without and with 1 wt % Cu were subjected to indirect extrusion processing in order to investigate the influence of addition of Cu on the microstructure and corrosion behavior in the extruded condition.

2. Experimental Procedure

The alloys with the nominal compositions of Mg–6 wt % Zn–0.5 wt % Zr (ZK60) and Mg–6 wt % Zn–0.5 wt % Zr–1 wt % Cu (ZKC601) were created by induction melting using the graphite crucibles under an inert atmosphere with a mixture of CO_2 and SF_6. The analyzed compositions of the alloys are given in Table 1. To cast a billet, each alloy was stabilized for 10 min in a molten state at 700 °C, before being poured into a steel mold that was pre-heated to 200 °C. After casting, the alloys were homogenized at 440 °C for 4 h, before being water-quenched. Each cylindrical billet has a diameter of 80 mm and a length of 150 mm. Indirect extrusion experiments were executed at a ram speed of 1.3 mm s^{-1}, an extrusion ratio of 25 and an initial billet temperature of 250 °C.

Table 1. Chemical compositions (wt %) of the ZK60 and ZKC601 alloys investigated in this study.

Alloy	Zn	Zr	Cu	Fe	Si	Mg
ZK60	5.50	0.58	<0.001	0.0026	0.0019	bal.
ZKC601	5.52	0.57	0.88	0.0029	0.0018	bal.

The microstructural examinations were carried out on the midsections that were parallel to the extrusion direction (ED) by a Quanta 200 field-emission scanning electron microscope (FEI, Hillsboro, OR, USA); a JEOL JXA-8530F energy probe microanalyzer (JEOL, Tokyo, Japan); and a JEM-2100F Cs-corrected transmission electron microscope (JEOL, Tokyo, Japan).

The samples prepared for microstructural analysis were ground with SiC papers (up to 1200 grit) under a fresh water atmosphere. The samples were subsequently polished using a diamond paste (1 μm) and a colloidal silica (0.04 μm) solution under a 95% ethanol atmosphere. A focused ion beam technique was used to fabricate the transmission electron microscopy (TEM) samples.

To investigate the corrosion properties of the extruded alloys, immersion tests, H_2 volume measurement and potentiodynamic polarization tests were conducted in a 0.6 M NaCl solution (1.0 L) at 25 °C. The cleaning of the sample after the immersion test was carried out with CrO_3 solution (200 g L^{-1}), before the weight loss was measured. The H_2 volume measurements were executed following the method proposed by Song and Atrens [15]. The data values obtained from these tests were averaged with the ones obtained from three repeated experiments. A potentiostat (Reference 600, GAMRY, Warminster, PA, USA) was used to conduct potentiodynamic polarization tests at a potential sweep rate of 2 mV s^{-1} in a 0.6 M NaCl solution after deaeration. A conventional three-electrode cell consisting of a saturated calomel reference electrode (SCE), a Pt plate counter electrode and a working electrode (sample) was used.

A scanning Kelvin probe force microscopy (SKPFM) (NT-MDT, Moscow, Russia) was used to see the Volta potential differences between the phases present in the extruded alloys. The Pt-coated conducting tip was modulated by the AC modulation of 0.3 V at 70 kHz, which was generated by a lock-in amplifier. All SKPFM measurements were conducted at the ambient temperature. The details of the corrosion-related tests and SKPFM measurement are available in previous studies [16,17].

3. Results and Discussion

3.1. Microstructure

Figure 1a,b show the scanning electron microscopy (SEM) micrographs of the extruded ZK60 and ZKC601 alloys, respectively. As reported previously, the ZK60 alloy contains Zn-containing particles, such as $MgZn_2$ and Zn_2Zr_3 in the α-Mg matrix [18–21]. On the other hand, three different types of Zn-containing particles can be distinguished in the Cu-added ZKC601 alloy, which is indicated by A, B and C in Figure 1b. The energy probe microanalysis results shown in Figure 1c–e reveal that particle A is highly rich in Cu, while particles B and C contain relatively small amounts of Cu. In addition,

particle B is considered different from particle C as the Zr content in the former is negligible, while the Zr content in the latter is relatively high.

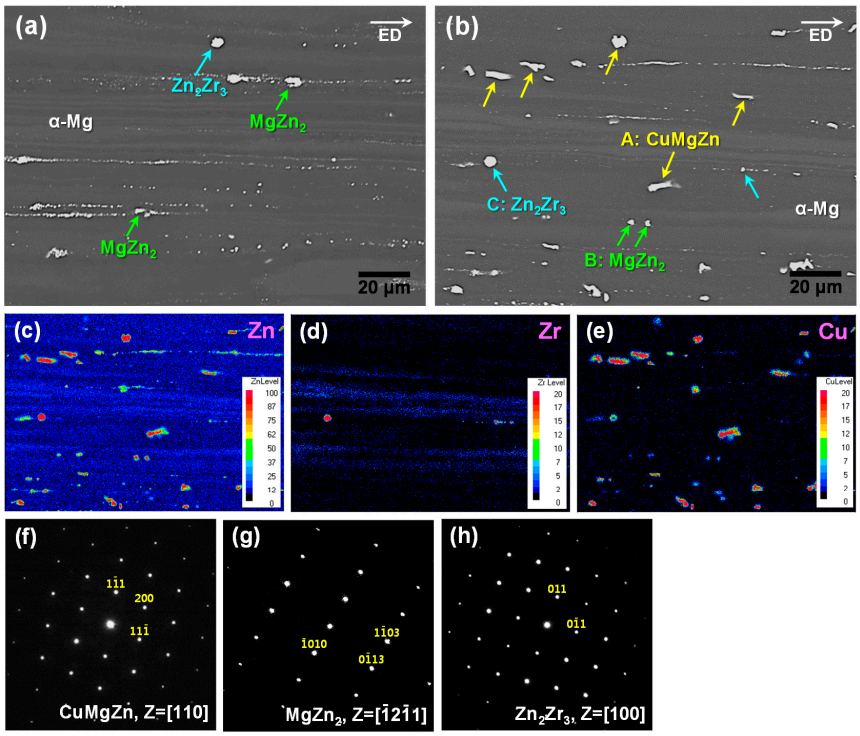

Figure 1. Scanning electron microscopy (SEM) micrographs of the extruded (**a**) ZK60 and (**b**) ZKC601 alloys; the energy probe microanalysis maps obtained from the ZKC601 alloy for (**c**) Zn, (**d**) Zr and (**e**) Cu; and electron beam diffraction patterns from (**f**) CuMgZn, (**g**) $MgZn_2$ and (**h**) Zn_2Zr_3 in the ZKC601 alloy.

Further TEM analysis with the electron beam diffraction patterns was conducted for the second-phase particles existing in the ZKC601 alloy, which is shown in Figure 1f–h. The highly Cu-rich phase (particle A) is well matched with CuMgZn, which has a face-centered cubic structure. The Zn-rich phase (particle B) is consistent with $MgZn_2$, which has a hexagonal close-packed structure. In addition, the Zr-rich phase (particle C) can be identified as Zn_2Zr_3, which has a tetragonal structure. Since the $MgZn_2$ and Zn_2Zr_3 particles are also visible in the ZK60 alloy, the addition of Cu to the ZK60 alloy results in the additional presence of CuMgZn particles in the extruded condition. It should be also noted that all of the intermetallic particles in the Cu-added ZKC601 alloy contain a certain amount of Cu, which does not occur in the ZK60 alloy without added Cu.

3.2. Corrosion Properties

The macroscopic corrosion development of the extruded alloys during the immersion in the 0.6 M NaCl solution at 25 °C is shown in Figure 2. Overall, the extruded alloys showed similar corrosion behavior as their corrosion initiates in the typical local corrosion mode, before propagating in the filiform corrosion mode. During the early stage of immersion for 10 min, both the alloys appeared to be free of local corrosion. However, after immersion for 30 min, severe corrosion started forming on the ZKC601 alloy, while localized corrosion appeared to initiate in the ZK60 alloy, which is indicative of faster corrosion development in the former than in the latter during the immersion tests.

Figure 3a provides the values of weight loss and collected the H_2 volume for the extruded alloys after immersion for 72 h in the 0.6 M NaCl solution. As indicated, the weight loss and the H_2 volume quantities of the ZKC601 alloy are larger than those of the ZK60 alloy, which indicated that the addition

of Cu to the latter has a detrimental effect on the corrosion resistance under the current corrosive conditions. The values of weight loss for 72 h were 10.92 ± 0.13 and 12.64 ± 0.21 mg cm^{-2}, while the amounts of collected H_2 volume for 72 h were 5.70 ± 0.18 and 7.07 ± 0.56 mL cm^{-2} for the ZK60 and ZKC601 alloys, respectively. The corrosion rates, which correspond to the weight loss values, are 7.21 ± 0.08 and 8.33 ± 0.14 mm $year^{-1}$ for the ZK60 and ZKC601 alloys, respectively.

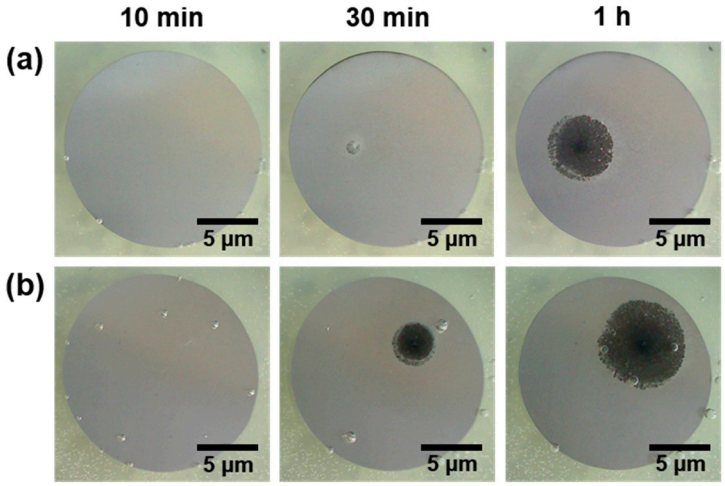

Figure 2. Optical micrographs showing the macroscopic surfaces of the extruded (**a**) ZK60 and (**b**) ZKC601 alloys after immersion for various times in 0.6 M NaCl solution at 25 °C.

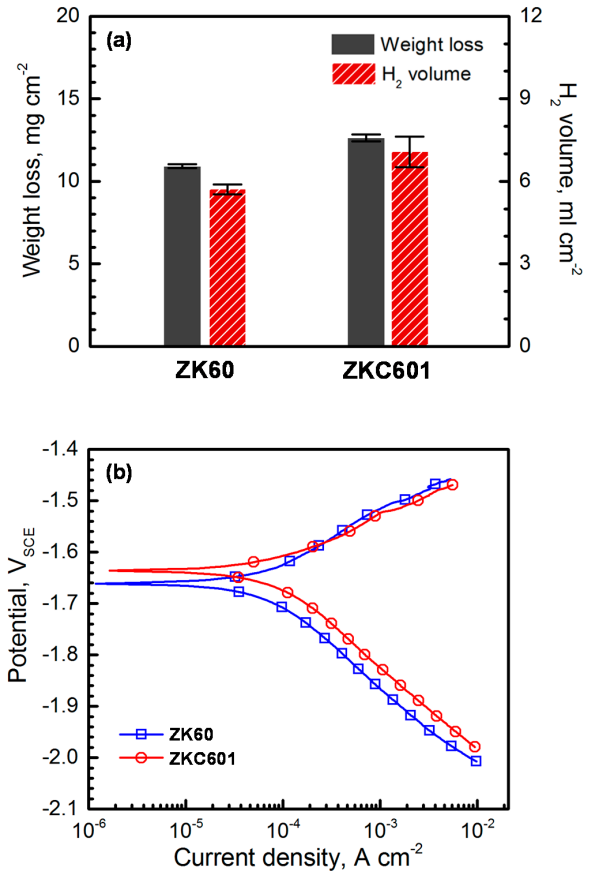

Figure 3. (**a**) Values of weight loss and collected H_2 volume after immersion for 72 h in 0.6 M NaCl solution and (**b**) potentiodynamic polarization curves of the ZK60 and ZKC601 alloys.

The potentiodynamic polarization curves of the ZK60 and ZKC601 alloys are shown in Figure 3b. First, the ZK60 alloy was found to have lower corrosion potential (E_{corr}) than the ZKC601 alloy as the ZK60 and ZKC601 alloys show the E_{corr} values of −1.66 and −1.64 V_{SCE}, respectively. The cathodic side of the curves indicates that the cathodic current density ($i_{cathodic}$) of the ZKC601 alloy is higher than that of the ZK60 alloy. For example, the $i_{cathodic}$ values at −1.75 V_{SCE} were −0.21 and −0.37 mA cm^{-2} for the ZK60 and ZKC601 alloys, respectively. However, it is clearly recognizable that the addition of Cu to the alloy has little influence on the anodic polarization behavior of the ZK60 alloy, indicating that the increased E_{corr} after Cu alloying results solely from an increase in $i_{cathodic}$.

3.3. Influence of Intermetallic Particles

Since the electrochemical potential differences between the α-Mg matrix and the intermetallic particles are considered to be an important factor affecting $i_{cathodic}$ and microgalvanic corrosion [22–24], Volta potential maps were obtained using SKPFM for the extruded ZK60 and ZKC601 alloys, which is shown in Figure 4. It was found that the intermetallic particles in the alloys have greater Volta potentials than the α-Mg matrix, indicating that the former is nobler than the latter. However, the Volta potential appears to differ depending on the type of intermetallic particles, which is typically observed. The $MgZn_2$ and Zn_2Zr_3 particles in the ZK60 alloy appeared to have Volta potentials that are about 320 and 230 mV higher than the α-Mg matrix, respectively. On the other hand, the CuMgZn, $MgZn_2$ and Zn_2Zr_3 particles in the ZKC601 alloy showed Volta potentials that were about 680, 510 and 370 mV higher than the α-Mg matrix, respectively. This demonstrates that the intermetallic particles existing in the ZKC601 alloy can be electrochemically nobler than those present in the ZK60 alloy, which is ascribed to the incorporation of Cu in the intermetallic particles of the ZKC601 alloy. The SKPFM results suggest that the ZKC601 alloy can be more susceptible to microgalvanic corrosion between the α-Mg matrix and the intermetallic particles compared to the ZK60 alloy in a corrosive environment.

A SEM micrograph showing the corroded surface of the ZKC601 alloy after immersion for 1 h in the 0.6 M NaCl solution is provided in Figure 5 to reveal the dependence of the corrosion development on the presence of intermetallic particles. As expected, severe corrosion preferentially occurred around CuMgZn particles, whereas such localized corrosion was not observed around the less noble Zn_2Zr_3 and $MgZn_2$ particles. This indicates that the presence of noble CuMgZn particles in the ZKC601 alloy can degrade its corrosion resistance by activating microgalvanic corrosion between the α-Mg matrix and the intermetallic particles.

3.4. Corrosion-Controlling Factor

In general, the deterioration of corrosion resistance can be understood by an increased H_2 evolution rate and/or degraded passivity [25–27]. Recently, it has been reported that the H_2 evolution rate is closely related with weight loss in the corrosion of Mg alloys [28–32]. As mentioned above, the ZKC601 alloy showed a corrosion rate that was 16% higher than that of the ZK60 alloy in the 0.6 M NaCl solution at 25 °C. Furthermore, the former alloy exhibited a generation of H_2 that was 24% greater than the latter alloy after 72 h in the NaCl solution. Furthermore, the polarization curves directly revealed that the addition of 1.0 wt % Cu to the ZK60 alloy results in an increase in $i_{cathodic}$. Therefore, it can be conceived that the increased corrosion rate after addition of Cu is closely associated with an increase in the H_2 evolution rate. However, the increased corrosion rate by addition of Cu is not likely to result from the degradation of passivity since the passive current density in the polarization curves does not show a clear dependence on the Cu content of the extruded alloys.

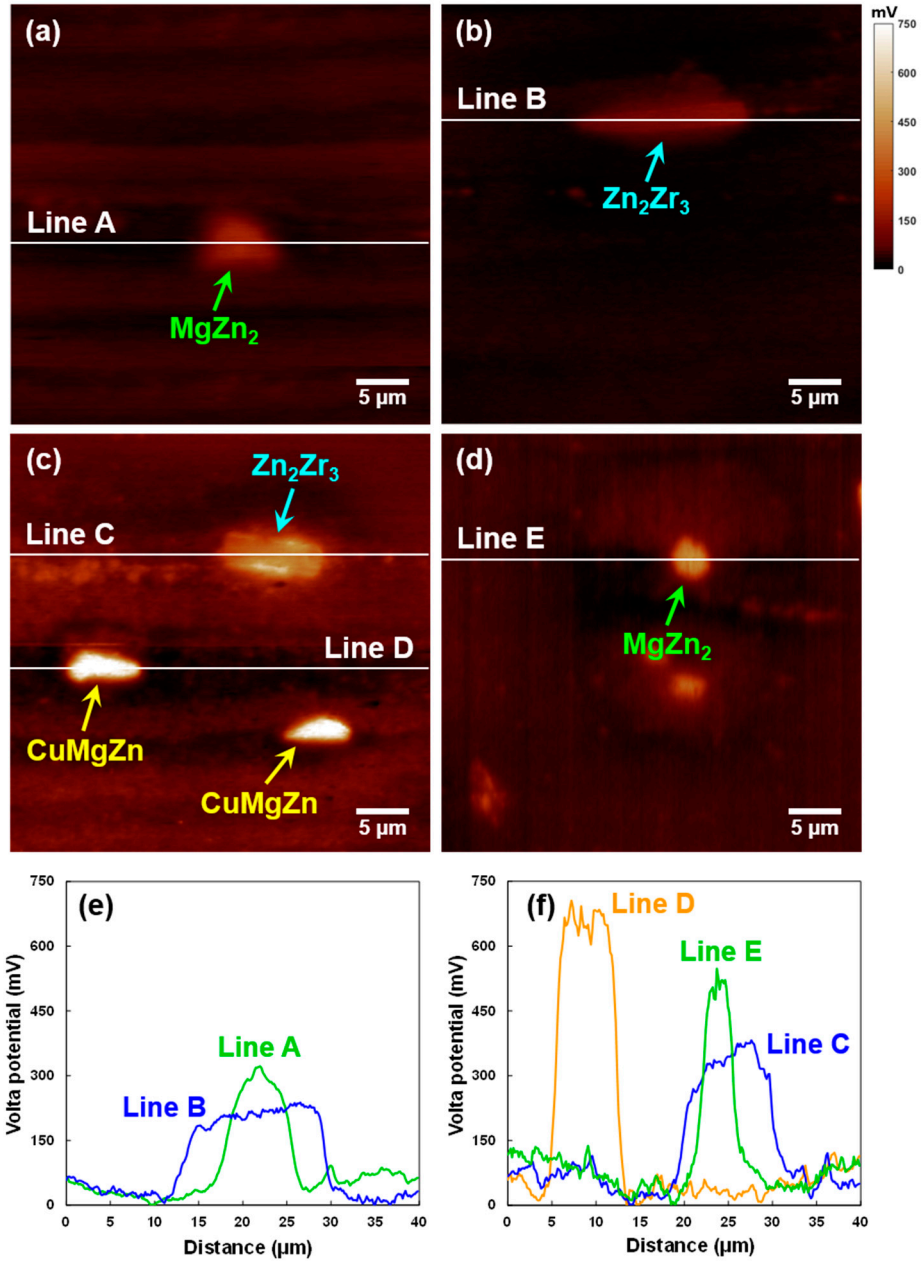

Figure 4. Scanning Kelvin probe force microscopy (SKPFM) images of the extruded (**a**,**b**) ZK60 and (**c**,**d**) ZKC601 alloys; and corresponding Volta potential profiles along the lines (**e**) A–B and lines (**f**) C–E in the SKPFM images.

With respect to a microstructural factor influencing the change in corrosion resistance, the H_2 evolution activated by addition of Cu can be attributed to the formation of electrochemically noble intermetallic particles, leading to the activation of microgalvanic corrosion. The SKPFM measurements indicated that the electrochemical nobility of intermetallic particles is enhanced by addition of Cu. This change in nobility occurred by the formation of highly noble CuMgZn particles and the incorporation of Cu into the $MgZn_2$ and Zn_2Zr_3 particles existing in the ZK60 alloy. As shown above, the presence of noble Cu-containing intermetallic particles enhances the microgalvanic corrosion, thereby leading to the relatively active H_2 evolution and corresponding fast corrosion rate in the ZKC601 alloy. On the other hand, the contribution of the alloyed Cu to enhancing the nobility of the

α-Mg matrix and hence, lowering its susceptibility to microgalvanic corrosion, is not expected due to the highly limited solid solubility of Cu in Mg [5,33].

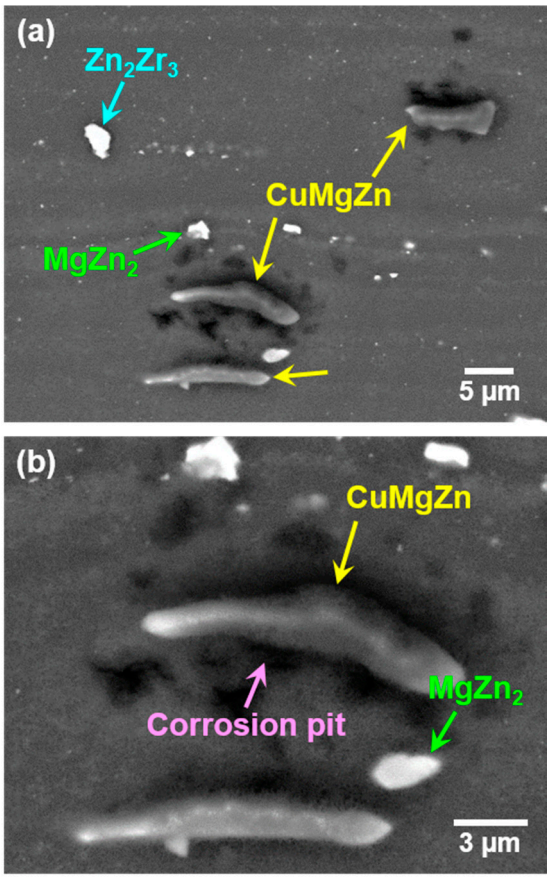

Figure 5. SEM micrographs showing the corroded surface of the ZKC601 alloy after immersion for 1 h in 0.6 M NaCl solution at 25 °C at relatively (**a**) low and (**b**) high magnifications.

4. Conclusions

The effect of 1 wt % addition of Cu on the microstructure and corrosion behavior of the ZK60 alloy subjected to indirect extrusion was investigated. The CuMgZn, $MgZn_2$ and Zn_2Zr_3 particles were found to exist in the Cu-added ZKC601 alloy, while only $MgZn_2$ and Zn_2Zr_3 particles were observable in the ZK60 alloy. The corrosion rates measured in a 0.6 M NaCl solution at 25 °C were found to be 7.21 and 8.33 mm year^{-1} for the ZK60 and ZKC601 alloys, respectively. The degraded corrosion resistance due to the addition of Cu is mainly attributed to the presence of noble CuMgZn particles, which contribute to the enhancement of microgalvanic corrosion.

Author Contributions: S.-M.B. and B.K. carried out sample preparation, microstructural investigation, and corrosion-related characterization using potentiodynamic polarization tests and immersion tests. S.S.P. conceived and designed the experiments. All the authors contributed to discussion and paper writing. S.-M.B. and B.K. contributed equally to this work.

Funding: This research received no external funding.

Acknowledgments: This work was supported by the 2018 Research Fund (2.180053.01) of UNIST (Ulsan National Institute of Science & Technology). The authors are grateful to Ki-Suk Lee and Sooseok Lee of UNIST for their experimental assistance in SKPFM measurement.

Conflicts of Interest: The authors declare no conflict of interest.

References

1. Bettles, C.J.; Gibson, M.A. Current wrought magnesium alloys: Strength and weakness. *JOM* **2005**, *57*, 46–49. [CrossRef]
2. Kim, N.J. Magnesium sheet alloys: Viable alternatives to steels? *Mater. Sci. Technol.* **2014**, *30*, 1925–1928. [CrossRef]
3. Davies, C.; Barnett, M. Expanding the extrusion limits of wrought magnesium alloys. *JOM* **2004**, *56*, 22–24. [CrossRef]
4. Peng, Z.; Sheppard, T. Study of surface cracking during extrusion of aluminium alloy AA 2014. *Mater. Sci. Technol.* **2004**, *20*, 1179–1191. [CrossRef]
5. Polmear, I.J. *Light Alloys*, 3rd ed.; Arnold: London, UK, 1995; pp. 219–221; ISBN 0-340-63207-0.
6. Park, S.H.; Yu, H.; Kim, H.S.; Bae, J.H.; Yim, C.D.; You, B.S. Effect of Cu addition on the microstructure and mechanical properties of an as-extruded ZK60 alloy. *Korean J. Met. Mater.* **2013**, *51*, 169–179. [CrossRef]
7. Buha, J. Mechanical properties of naturally aged Mg–Zn–Cu–Mn alloy. *Mater. Sci. Eng. A* **2008**, *489*, 127–137. [CrossRef]
8. Zhu, H.M.; Sha, G.; Liu, J.W.; Wu, C.L.; Luo, C.P.; Liu, Z.W.; Zheng, R.K.; Ringer, S.P. Microstructure and mechanical properties of Mg–6Zn–xCu–0.6Zr (wt %) alloys. *J. Alloy. Compd.* **2011**, *509*, 3526–3531. [CrossRef]
9. Yu, H.; Yu, H.S.; Kim, Y.M.; You, B.S.; Min, G.H. Hot deformation behavior and processing maps of Mg–Zn–Cu–Zr magnesium alloy. *Trans. Nonferr. Met. Soc.* **2013**, *23*, 756–764. [CrossRef]
10. Zhu, H.M.; Luo, C.P.; Liu, J.W.; Jiao, D.L. Effects of Cu addition on microstructure and mechanical properties of as-cast magnesium alloy ZK60. *Trans. Nonferr. Met. Soc.* **2014**, *24*, 605–610. [CrossRef]
11. Hanawalt, J.D.; Nelson, C.E.; Peloubet, J.A. Corrosion studies of magnesium and its alloys. *Trans. AIME* **1942**, *147*, 273–299.
12. Hillis, J.E.; Reichek, K.N. *High. Purity Magnesium AM60 Alloy.: The Critical Contaminant Limits and the Salt Water Corrosion Performance*; SAE Technical Paper; Society of Automotive Engineers: Detroit, MI, USA, 1986; p. 860288.
13. Song, G.; Atrens, A. Corrosion mechanisms of magnesium alloys. *Adv. Eng. Mater.* **1999**, *1*, 11–33. [CrossRef]
14. Budruk Abhijeet, S.; Balasubramaniam, R.; Gupta, M. Corrosion behavior of Mg–Cu and Mg–Mo composites in 3.5% NaCl. *Corros. Sci.* **2008**, *50*, 2423–2428. [CrossRef]
15. Song, G.; Atrens, A. Understanding magnesium corrosion. *Adv. Eng. Mater.* **2003**, *5*, 837–858. [CrossRef]
16. Kim, H.J.; Kim, B.; Baek, S.-M.; Sohn, S.-D.; Shin, H.-J.; Jeong, H.Y.; Yim, C.D.; You, B.S.; Ha, H.-Y.; Park, S.S. Influence of alloyed Al on the microstructure and corrosion properties of extruded Mg–8Sn–1Zn alloys. *Corros. Sci.* **2015**, *95*, 133–142. [CrossRef]
17. Baek, S.-M.; Kim, H.J.; Jeong, H.Y.; Sohn, S.-D.; Shin, H.-J.; Choi, K.-J.; Lee, K.-S.; Lee, J.G.; Yim, C.D.; You, B.S.; et al. Effect of alloyed Ca on the microstructure and corrosion properties of extruded AZ61 Mg alloy. *Corros. Sci.* **2016**, *112*, 44–53. [CrossRef]
18. Galiyev, A.; Kaibyshev, R.; Gottstein, G. Correlation of plastic deformation and dynamic recrystallization in magnesium alloy ZK60. *Acta Mater.* **2001**, *49*, 1199–1207. [CrossRef]
19. Ma, C.J.; Liu, M.; Wu, G.H.; Ding, W.J.; Zhu, Y.P. Microstructure and mechanical properties of extruded ZK60 magnesium alloy containing rare earth. *Mater. Sci. Technol.* **2004**, *20*, 1661–1665. [CrossRef]
20. Wang, H.-Y.; Rong, J.; Yu, Z.-Y.; Zha, M.; Wang, C.; Yang, Z.-Z.; Bu, R.-Y.; Jiang, Q.-C. Tensile properties, texture evolution and deformation anisotropy of as-extruded Mg–6Zn–1Zr magnesium alloy at room and elevated temperatures. *Mater. Sci. Eng. A* **2017**, *697*, 149–157. [CrossRef]
21. Yang, Y.; Wang, Z.; Jiang, L. Evolution of precipitates in ZK60 magnesium alloy during high strain rate deformation. *J. Alloy. Compd.* **2017**, *705*, 566–571. [CrossRef]
22. De Wit, J.H.W. Local potential measurements with the SKPFM on aluminium alloys. *Electrochim. Acta* **2004**, *49*, 2841–2850. [CrossRef]
23. Coy, A.E.; Viejo, F.; Skeldon, P.; Thompson, G.E. Susceptibility of rare-earth-magnesium alloys to micro-galvanic corrosion. *Corros. Sci.* **2010**, *52*, 3896–3906. [CrossRef]
24. Hurley, M.F.; Efaw, C.M.; Davis, P.H.; Croteau, J.R.; Graugnard, E.; Birbilis, N. Volta potentials measured by scanning Kelvin probe force microscopy as relevant to corrosion of magnesium alloys. *Corrosion* **2015**, *71*, 160–170. [CrossRef]

25. Esmaily, M.; Blücher, D.B.; Svensson, J.E.; Halvarsson, M.; Johansson, L.G. New insights into the corrosion of magnesium alloys—The role of aluminum. *Scr. Mater.* **2016**, *115*, 91–95. [CrossRef]
26. Ha, H.-Y.; Kim, H.J.; Baek, S.-M.; Kim, B.; Sohn, S.-D.; Shin, H.-J.; Jeong, H.Y.; Park, S.H.; Yim, C.D.; You, B.S.; et al. Improved corrosion resistance of extruded Mg–8Sn–1Zn–1Al alloy by microalloying with Mn. *Scr. Mater.* **2015**, *109*, 38–43. [CrossRef]
27. Ha, H.-Y.; Kang, J.-Y.; Yang, J.; Yim, C.D.; You, B.S. Role of Sn in corrosion and passive behavior of extruded Mg–5 wt % Sn alloy. *Corros. Sci.* **2016**, *102*, 355–362. [CrossRef]
28. Birbilis, N.; Williams, G.; Gusieva, K.; Samaniego, A.; Gibson, M.A.; McMurray, H.N. Poisoning the corrosion of magnesium. *Electrochem. Commun.* **2013**, *34*, 295–298. [CrossRef]
29. Ha, H.-Y.; Kang, J.-Y.; Yang, J.; Yim, C.D.; You, B.S. Limitations in the use of the potentiodynamic polarisation curves to investigate the effect of Zn on the corrosion behaviour of as-extruded Mg–Zn binary alloy. *Corros. Sci.* **2013**, *75*, 426–433. [CrossRef]
30. Ha, H.-Y.; Kang, J.-Y.; Kim, S.G.; Kim, B.; Park, S.S.; Yim, C.D.; You, B.S. Influences of metallurgical factors on the corrosion behaviour of extruded binary Mg–Sn alloys. *Corros. Sci.* **2014**, *82*, 369–379. [CrossRef]
31. Ha, H.-Y.; Kang, J.-Y.; Yim, C.D.; Yang, J.; You, B.S. Role of hydrogen evolution rate in determining the corrosion rate of extruded Mg–5Sn–(1–4 wt %)Zn alloys. *Corros. Sci.* **2014**, *89*, 275–285. [CrossRef]
32. Baek, S.-M.; Kang, J.S.; Shin, H.-J.; Yim, C.D.; You, B.S.; Ha, H.-Y.; Park, S.S. Role of alloyed Y in improving the corrosion resistance of extruded Mg–Al–Ca-based alloy. *Corros. Sci.* **2017**, *118*, 227–232. [CrossRef]
33. Cao, F.; Song, G.-L.; Atrens, A. Corrosion and passivation of magnesium alloys. *Corros. Sci.* **2016**, *111*, 835–845. [CrossRef]